Available online at www.sciencedirect.com

ScienceDirect

Ceramics International 39 (2013) 8823–8831

CERAMICS INTERNATIONAL

www.elsevier.com/locate/ceramint

Influence of reactant type on the Sr incorporation grade and structural characteristics of $Ba_{1-x}Sr_xTiO_3$ ($x=0-1$) grown by sol–gel-hydrothermal synthesis

S. Fuentes[a,f,*], E. Chávez[b,c], L. Padilla-Campos[d], D.E. Diaz-Droguett[e]

[a]Departamento de Ciencias Farmacéuticas, Facultad de Ciencias, Universidad Católica del Norte, Casilla 1280, Antofagasta, Chile
[b]Department of Physics, Universitat Autònoma de Barcelona, Campus de la UAB, 08193 Bellaterra (Barcelona), Spain
[c]Catalan Institute of Nanotechnology (ICN-CIN2), Campus de la UAB 08193 Bellaterra (Barcelona), Spain
[d]Departamento de Química, Facultad de Ciencias Básicas, Universidad de Antofagasta, Casilla 170, Antofagasta, Chile
[e]Departamento de Física, Facultad de Física, Pontificia Universidad Católica de Chile, Casilla 306, Santiago, Chile
[f]Center for the Development of Nanoscience and Nanotechnology, CEDENNA, Santiago, Chile

Received 11 February 2013; received in revised form 19 April 2013; accepted 20 April 2013
Available online 27 April 2013

Abstract

The influence of barium and strontium starting reactants used in different mole ratios, $BaCl_2$ and $Ba(OH)_2$, $SrCl_2$ and $Sr(OH)_2$, on the chemical and structural properties of $Ba_{1-x}Sr_xTiO_3$ ($x=0-1$) (BST) nanoparticles prepared via sol–gel-hydrothermal synthesis in an oxygen atmosphere is discussed. The effect of the type of reactant on the relative amount of Sr incorporated in BST compound was also analysed. The synthesised BST nanoparticles showed differences in their structural and chemical characteristics, which were attributed to the presence of Cl^- or OH^- anions during the synthesis of the compound. The structure, morphology and oxidation state of the samples were studied by X-ray diffraction, transmission electron microscopy and X-ray photoelectron spectroscopy, respectively. In addition, theoretical calculations using cluster models were carried out to understand the possible phases formed of BST, the effect of the Sr incorporation and the possible presence of oxygen vacancies inside the BST structure.

Keywords: A. Sol–gel processes; B. Defects; B. Spectroscopy; C. Ferroelectric properties; D. $BaTiO_3$ and titanates

1. Introduction

Ferroelectric materials are used in many modern devices, such as piezoelectric actuators and electro-optic modulators. Materials of the ABO_3 family (A and B are cations and O is oxygen), such as $BaTiO_3$, $PbTiO_3$ and $SrTiO_3$, have received a significant amount of attention due to their ferroelectric and electro-optic properties [1–3]. The properties and behaviour of macroscopic ferroelectric materials are well known.

More recently, the investigation of properties has been extended to the electronic structures of the impurities, surfaces, and electron-doped $SrTiO_3$ (ST) or $BaTiO_3$ (BT) [4,5]. However, the atomic structure and the electronic properties of the grain boundaries in $BaTiO_3$ or $SrTiO_3$ are the subject of great interest due to their technological implications. There are various reports on the effects of impurity doping on the properties of this interesting system [6].

Among other materials, barium strontium titanate, $BaSrTiO_3$ or BST, is the most extensively studied perovskite ferroelectric oxide. This material is invaluable for the electronics industry, due to its high dielectric constant, low dielectric loss, good thermal stability and high frequency characteristics [7,8]. BT and BST are commonly used in a number of electronic devices such as transducers, piezoelectric actuators, thermal switches, passive memory storage devices and dynamic random access memories (DRAMs) [9,10]. The properties of BST strongly depend on the composition and characteristics of its constituent materials; therefore, efforts are still in progress to synthesise BST compounds with excellent properties.

*Corresponding author at: Universidad Católica del Norte, Departamento de Ciencias Farmacéuticas, Facultad de Ciencias, Av. Angamos 0610, Antofagasta, Chile. Tel.: +56 55 355383; fax: +56 55 355632.
E-mail address: sfuentes@ucn.cl (S. Fuentes).

0272-8842/$ - see front matter © 2013 Elsevier Ltd and Techna Group S.r.l. All rights reserved.
http://dx.doi.org/10.1016/j.ceramint.2013.04.070

Barium strontium titanate, $Ba_xSr_{1-x}TiO_3$, is a solid solution of $BaTiO_3$ and $SrTiO_3$. At room temperature, $BaTiO_3$ and Ba-rich $Ba_xSr_{1-x}TiO_3$ compounds have a tetragonal lattice and are ferroelectric, whereas $SrTiO_3$ and Sr-rich $Ba_xSr_{1-x}TiO_3$ compounds are cubic and paraelectric. The substitution of Ba by Sr will result in a decrease of the Curie temperature and an increase in the dielectric constant of the material [11].

Several methods have been considered for the preparation of BST in powder form, including the sol–gel method [12], a solid-state reaction [13], spray pyrolysis [14], combustion synthesis [15], a microwave method [16] and a hydrothermal method [17,18]. The latter method is advantageous due to low temperature processing, the non-vacuum requirement and a low cost compared with others.

In ferroelectric fine particles, ferroelectricity decreases with decreasing particle grain size and disappears below a certain critical size [19,20]. Other physicochemical factors, such as the density, shape, presence of impurities and structural defects, also affect this property [21,22]. Moreover, Dutta et al. [23] have proposed that a relationship exists between the tetragonality in BT and the type of counter ion used in the synthesis. Although the exact mechanism of this process is not yet known, the authors suggested that most soluble salts can promote the dissolution of BT, disturbing the dissolution–recrystallisation process. Thus, a better understanding of the structure-property relationship of perovskite nanocrystals is highly desirable, which is also necessary for developing high-performance electronic devices.

The structural and morphological characteristics of sol–gel-hydrothermal BST powders often vary as a function of the synthesis parameters, such as reaction time, reaction temperature, and composition. Thus, the study of how these parameters influence the BST composition is considered important, first to explain the fundamental crystallisation process and second to optimise the material properties for potential technological applications.

In the present study, we prepared barium strontium titanate ($Ba_{1-x}Sr_xTiO_3$, $x=0-1$) powders of nanoparticle size using the sol–gel-hydrothermal method with tetrachloride titanate and two sources of barium and strontium salts as the starting material at a typical temperature of 180 °C and 24 h of reaction time in an oxygen atmosphere. The effect of the synthesis conditions (presence of chloride ions and alkali metal ions) and the different mole ratios and on the characteristics of the resulting compound is analysed. Finally, theoretical calculations were carried out to help with the interpretation of the experimental results.

2. Experimental

$Ba_{1-x}Sr_xTiO_3$ powders prepared using a different Ba:Sr mole ratio ($x=0$, 0.3, 0.5, 0.8 and 1) were synthesised using the sol–gel-hydrothermal process with tetrachloride titanate ($TiCl_4$, 1 M) and two different salts of barium ($BaCl_2$, $Ba(OH)_2$) and strontium ($SrCl_2$, $Sr(OH)_2$) as the starting materials using two methods of synthesis.

Table 1
The preparing parameters of BST powders synthesized at 180 °C and 24 h.

Samples Method 1 (M1)	Ba:Sr in reactant	Samples Method 2 (M2)	Ba:Sr in reactant
B1	1:0	S1	1:0
B2	0.7:0.3	S2	0.7:0.3
B3	0.5:0.5	S3	0.5:0.5
B4	0.2:0.8	S4	0.2:0.8
B5	0:1	S5	0:1

In method 1 (M1), a typical synthesis of sample (B2) used $BaCl_2{\bullet}2H_2O$ (99.999%, Aldrich) and $SrCl_2{\bullet}6H_2O$ (99.995%, Aldrich) as the reactants (Table 1). A 1.1 mL solution (A) of $TiCl_4$ (1 M, Aldrich) was diluted in 2.3 mL of 2 M HCl to form a yellowish solution. The aqueous solution (B) was prepared by dissolving 0.52 g of $BaCl_2{\bullet}2H_2O$ and 0.4 g of $SrCl_2{\bullet}2H_2O$ in 20 mL of deionised water. For preparing the $BaSrTiO_3$ precursor, solution (B) was added into solution (A) with vigorous stirring for 1 h. Under stirring and N_2 bubbling, 13 mL of 6 M NaOH were added to the barium strontium titanium solution and a white homogeneous colloidal slurry (barium strontium titanium) was formed.

The mixed solution was transferred into a 100 mL Teflon-lined stainless steel reactor; the reactor was sealed and then heated for 24 h at 180 °C under a partial oxygen pressure of 60 psi. At the end of the reaction, the autoclave was naturally cooled to room temperature. The as-formed white solid powder that was attached to the bottom and inner wall of the Teflon container was collected, centrifuged, washed with distilled water and ethanol to remove the remaining ions, and dried at 60 °C for 6 h in vacuum.

In method 2 (M2), similarly, $Ba_{1-x}Sr_xTiO_3$ powders using the same Ba:Sr mole ratio were prepared using $Ba(OH)_2$ and $Sr(OH)_2$ as the starting materials (Table 1).

2.1. Characterisation

X-ray diffraction (XRD) data were acquired using a Siemens Advanced D-8 diffractometer with CuK_α radiation at 40 kV and 30 mA. Transmission electron microscopy (TEM) studies were performed in a Jeol JEM-2011 operated at 200 kV under diffraction and phase contrast modes. The surface chemical information of the samples was obtained by the X-ray photoelectron spectroscopy (XPS; Physical Electronics system model 1257) using an AlK_α emission. The binding energies and oxidation states were obtained from high-resolution scans. The energy scale was calibrated by assigning 284.8 eV to the C 1s peak, corresponding to adventitious carbon.

3. Results

3.1. X-ray diffraction

Fig. 1 shows the XRD patterns of the BST sample synthesised by the two methods (M1 and M2). As shown in Fig. 1a (M1) and c (M2), the sharp and well-defined peaks revealed high crystallinity

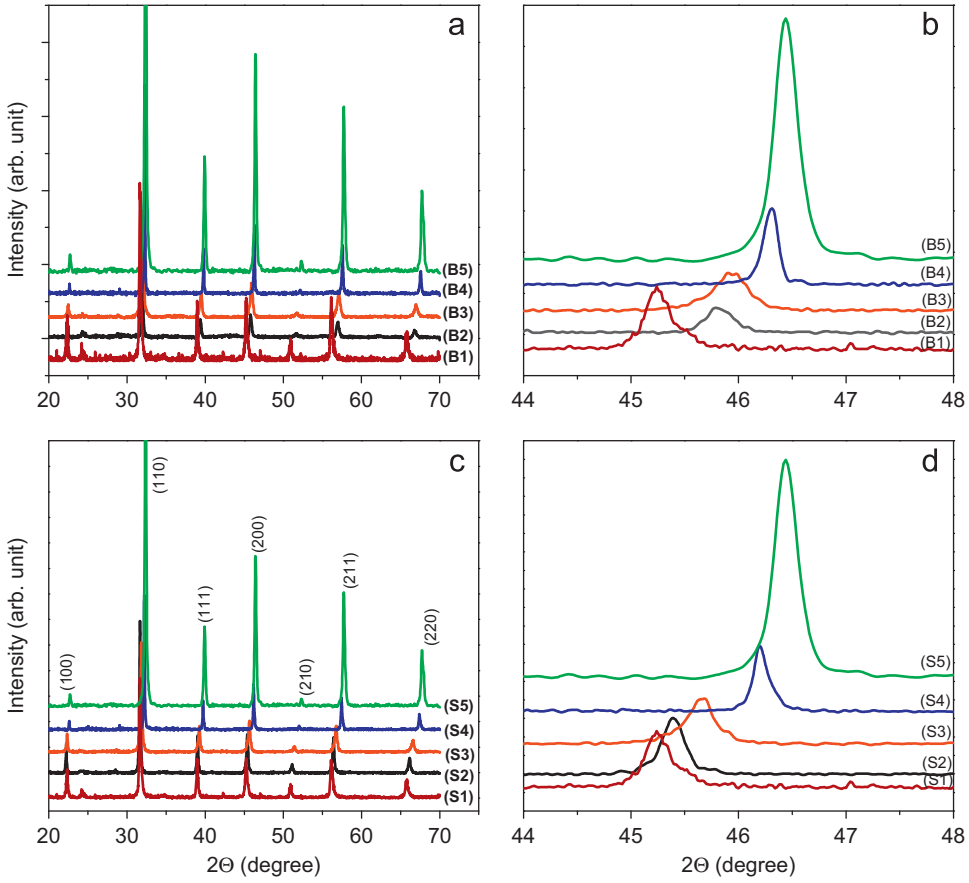

Fig. 1. XRD patterns of the product obtained with 24 h and 180 °C at different methods: (a) M1 in 2θ=20–70°, (b) M1 in 2θ=44–48, (c) M2 in 2θ=20–70, and (d) M2 in 2θ=44–48. The samples B1(S1) to B5(S5) of the $Ba_{1-x}Sr_xTiO_3$ compound correspond to synthesized samples from method M1(M2) with x=0, 0.3, 0.5, 0.8 and 1.0.

for all as-prepared BST powders which were not submitted to any heat treatment. The XRD Bragg's reflection was assigned to a cubic perovskite structure of BST. The absence of multiple sets of peaks, as suggested by other authors, indicated that not all the samples were phase-separated (barium-rich and strontium-rich phases), regardless of the Ba/Sr mole ratio and the method used to synthesise the samples [24].

In fact, all of the main peaks for the samples B1 and S1 (BT), as shown in Fig. 1, are apparently stabilised in the cubic lattice (space group *Pm3m*) for the BT powders at room temperature. The calculated lattice constants were in accordance with the tabulated values (a=4.0260; JCPDS card no. 31-0174). Several reasons have been proposed to explain the room temperature stabilisation of the cubic phase of BT powders, such as the presence of lattice 'defects' caused by hydroxyl ions, which are associated with powders formed via wet chemical methods, small deviations in Ba/Ti stoichiometry, or excess surface energy associated with ultrafine particles, among others [25]. Recently, our group reported that BT synthesised under similar conditions showed a cubic lattice and a strong peak at 307 cm^{-1} in its Raman spectrum, which is typical for the formation of a tetragonal or pseudo cubic phase with a slightly tetragonal distortion, which contradicted the results given by XRD [26].

Similarly, for samples B5 and S5, the peaks can also be indexed as a cubic lattice (space group *Pm3m*) of ST powders, and the calculated lattice constants were in good agreement with the tabulated values (a=3.9112 Å; JCPDS card no. 73-0661).

Table 2
Structural parameters of $BaSrTiO_3$ powders.

Samples Method 1 (M1)	2θ (2 0 0)	Samples Method 2 (M2)	2θ (2 0 0)
B1	45.25	S1	45.24
B2	45.80	S2	45.39
B3	45.94	S3	45.66
B4	46.31	S4	46.19
B5	46.45	S5	46.44

Fig. 1b and d shows the XRD patterns in the 44–48° 2θ range for all of the samples. A single diffraction peak between 45° and 47° is observed that corresponds to the (2 0 0) Bragg reflection, which is characteristic of the cubic lattice of BT and BST.

The effect of Sr substitution on the BT structure (B1 and S1) can be exemplified by the clear shifting of the (2 0 0) reflection. In both methods of BST preparation (M1 and M2), a shift was observed in the (2 0 0) peaks towards a high angle, compared with the position of the peak for pure BT (sample B1 and S1).

It is well known that this peak shift was due to the substitution of larger Ba^{2+} ions with smaller Sr^{2+} ions [17]. Table 2 shows that, under similar conditions, there is a greater

shift in the BST prepared using chloride ions in comparison with hydroxide ions of Ba^{2+} and Sr^{2+}.

3.2. Transmission electron microscopy

TEM images of the BST particles from B4 and S4 samples are shown in Fig. 2a and b. In general, the samples prepared under methods M1 and M2 show agglomerates of particles, 120–140 nm and 250–300 nm, respectively, which are composed of tight aggregates of several smaller nanoparticles.

Spherical particles of 120–300 nm were observed to gradually convert into aggregates of very fine particles. Notably, this type of disintegration is usually related to the hydroxylation in the sol–gel process in the early stage of hydrolysis. The formation of BST crystallites then occurs inside these aggregates because the diffusion distance is decreased and the driving force is locally increased by the presence of particles with a lower radius of curvature.

3.3. X-ray photoelectron spectroscopy

For a better characterisation of the local chemical environment of the BST compounds, high-resolution XPS spectra of the photoelectron signals of Ba, Sr, Ti, and O elements were acquired. Fig. 3(a–h) shows the spectra of Ba 3d, Sr 3d, Ti 2p and O 1s levels for the B4 and S4 samples.

Fig. 3a and b shows the Ba 3d doublet with binding energies of approximately 780 and 795 eV for the $3d_{5/2}$ and $3d_{3/2}$ peaks, respectively. In both samples, the values of the binding energies correspond to Ba atoms in the non-perovskite structure of BST, which is also called the decomposed perovskite structure or β-component of Ba [27].

Fig. 3c and d shows the Sr 3d levels, in which a more defined doublet was found for the S4 sample. The best fit assigned binding energies of 133.4 and 135.2 eV to the $3d_{5/2}$ and $3d_{3/2}$ peaks, respectively. These values for strontium in the B4 sample are attributed to a β-Sr form, whereas the values of the binding energies in the S4 sample of 132.7 and 134.5 eV for the $3d_{5/2}$ and $3d_{3/2}$ levels, respectively, correspond to α-Sr [27]. Here, the α-component corresponds to Sr atoms in the 'perovskite-like superconductor phase' BST structure.

The Ti 2p spectra (Fig. 3e and f) reveals binding energies of 458.7 eV ($2p_{3/2}$) and 464.5 eV ($2p_{1/2}$) for the sample B4, and 458.4 eV ($2p_{3/2}$) and 464.1 eV ($2p_{1/2}$) for the sample S4. These binding energies are close to the reported values for α-Ti atoms in the perovskite structure of BST and correspond to Ti in the +4 oxidation state [28]. The binding energies of the weak peaks of 457.0 ($2p_{3/2}$) and 462.7 eV ($2p_{1/2}$) of the sample B4 and 456.7 ($2p_{3/2}$) and 462.3 eV ($2p_{1/2}$) of the sample S4 were attributed to Ti^{3+} ions [28,29]. These ions correspond to a Ti_2O_3 (Ti^{3+}) compound, which is related to the non-perovskite structure of BST. Peaks attributed to TiO (Ti^{2+}) with binding energy for $Ti2p_{3/2}$ between 455 and 456 eV [28,29] were not detected in either sample.

Fig. 3g and h shows the O 1 s peak, which was fitted with two curves. The lower binding energy of 530.4 eV (B4) and 529.9 eV (S4) is attributed to O^{2-} ions in the perovskite structure of BST, indicating that the oxygen ions remain coordinated in TiO_6 octahedra [29]. On the other hand, the binding energies of 532.3 (B4) and 531.6 eV (S4) are attributed to a state O^{x-} ($0 < x < 2$), corresponding to chemisorbed species as well as oxygen vacancies. This variation in the chemical state of O is accompanied by that of Ti and could be related to the intermediate compounds of Ti_2O_3 and TiO; oxygen atoms in O^{x-} are also ascribed to the non-perovskite structure of BST [30]. After the fit performed on the O 1 s signal from all of the samples, it is important to highlight that more intense peaks associated with the oxidation state O^{x-} were found in the M1 method-grown samples than in the M2 method-grown samples. An example of that is revealed by Fig. 3g and h, where a lower intensity ratio between the O^{2-} and O^{x-} peaks is found for the B4 sample prepared using chloride ions compared with the S4 sample using hydroxide ions.

It has been reported [28] that changes in the O oxidation state are strongly associated with Ti oxidation changes (Ti^{+2} or Ti^{+3}), showing that a large concentration of O vacancies in the structure of the compound can exit. In our case, XPS analysis shows the presence of Ti^{+3}; therefore, oxygen vacancies are possible in the structure (see Fig. 3e and f).

The effect of the preparation methods (M1 and M2) on the Sr/Ba ratios in the BST samples are shown in Fig. 4. These values were calculated from XPS signals using the intensities ratio, I_{Sr3d}:I_{Ba3d}, and the ratio of the areas under the curve, A_{Sr3d}:A_{Ba3d}. The M2 method is more effective in the

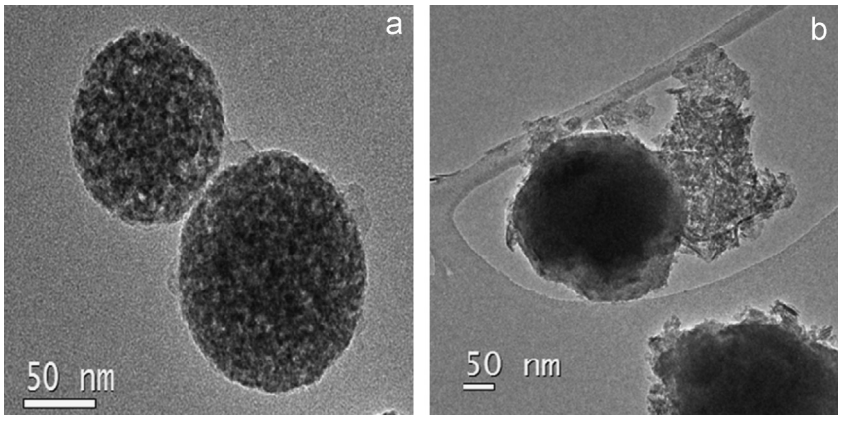

Fig. 2. TEM images of BST samples for both methods: (a) B4 and (b) S4.

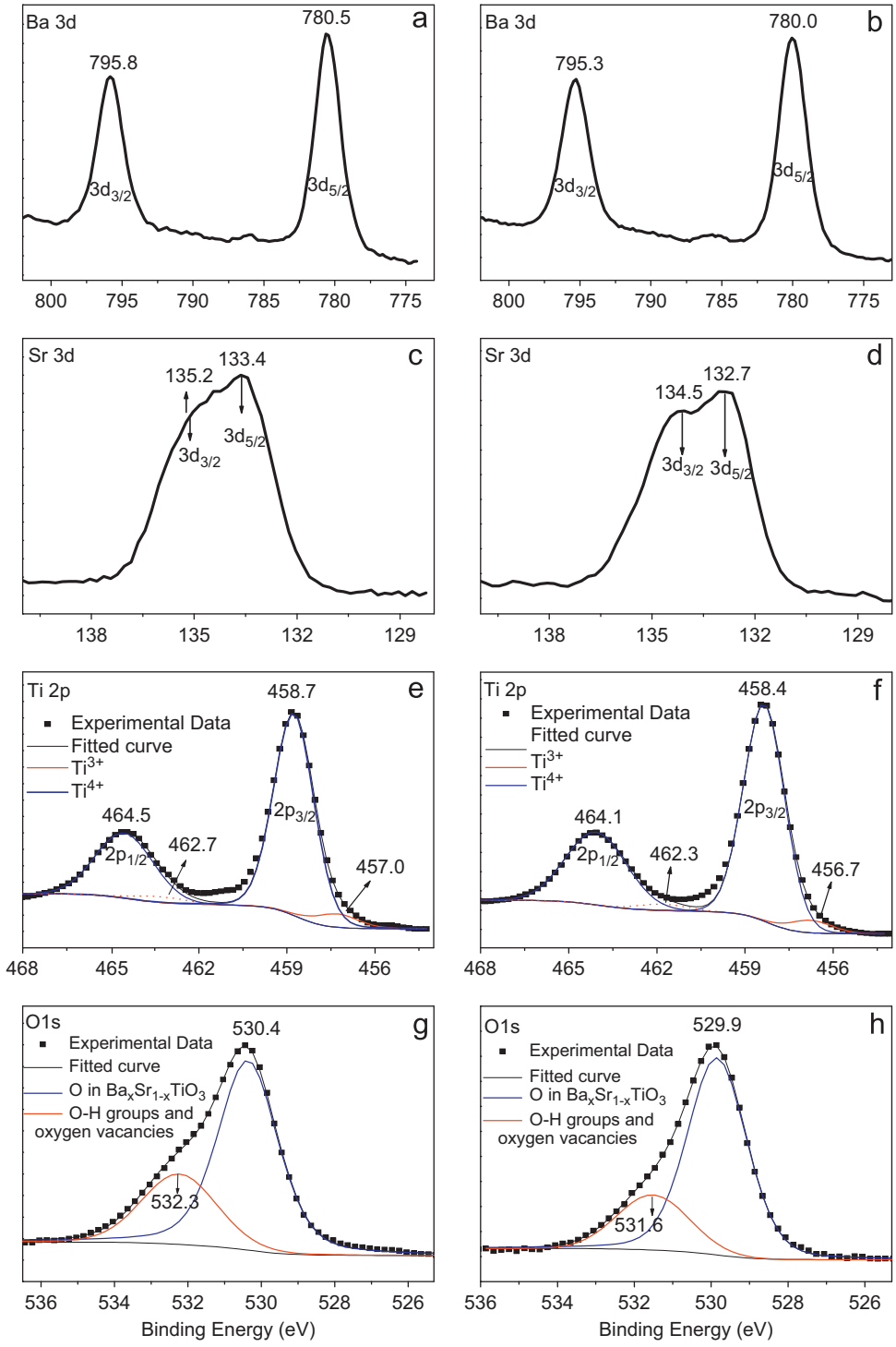

Fig. 3. XPS spectra of the elements for BST samples. Ba 3d doublet: (a) B4 and (b) S4; Sr 3d doublet: (c) B4 and (d) S4; O 1s: (e) B4 and (f) S4 and Ti 2p: (g) B4 and (h) S4.

incorporation of Sr^{2+} cations in the network of BT (S2 and S3) compared with samples B2 and B3 prepared under the M1 method ($x \leq 0.5$).

However, in the final stage of incorporation ($x \geq 0.5$) of Sr^{2+} for Ba^{2+}, there was a difference between the two methods (B4 and S4). Sample B4 had a higher proportion of Sr vs. Ba cations compared with sample S4. The higher ratios of intensity (0.18) and area under the curve (0.14) would indicate that the M1 method is now more effective in incorporating strontium into the lattice of BT.

4. Experimental discussion

The existence of preferential incorporation of strontium into the lattice of BT to form BST is well known. The formation of ST is thermodynamically more favourable than that of BT,

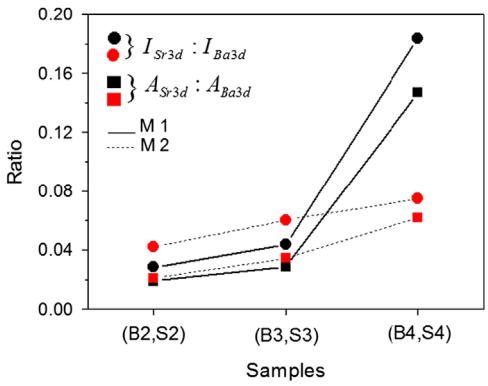

Fig. 4. Relative proportions coefficient of BST samples for both methods.

independent of the methods used. Another fact is that ST is more stable than BT at lower M cation concentrations (M=Sr or Ba) [31]. Our results indicate that the presence of anions in the reactant composition significantly influences the incorporation of strontium into the lattice of BT when x ≥0.5.

Furthermore, Dutta et al. [23] reported that the presence of anions in the reactant composition influences the particle size and tetragonal content of BT during synthesis in the following order: $I^- \sim Br^- \sim Cl^- > CH_3COO^- > NO_3^- > OH^-$. The anions perturb the dissolution–recrystallisation process, although the exact mechanism is not yet understood. Additionally, the mechanism for the influence of OH^- groups or Cl^- ions in the perovskite structure of BST under partial oxygen pressure has not been reported yet.

On the other hand, it was reported [32] that a sol–gel reaction between $Ti(OPr)_4$ and OH^- gives rise to a hexahydroxo titanate species ($[Ti(OH)_6]^{2-}$) as an intermediate, which is then condensed into stable $BaTiO_3$ with perovskite structure.

In agreement with Hua et al. [33], although without direct experimental evidence in the formation of $Ba[Ti(OH)_6]$, the formation of the hexahydroxo titanate species ($[Ti(OH)_6]^{2-}$) under strong alkaline conditions is possible. Therefore, an excess of OH^- will be required to produce the hexahydroxo titanate species ($[Ti(OH)_6]^{2-}$), which is the backbone of the TiO_6 octahedra. The different arrangements of the $[TiO_6]$ octahedra produce different polymorphic forms with different structures and properties, which could be related to the coordination group of Ti (IV) complex ion.

In our work, the total concentration of hydroxide ions present in the solution, using the M2 method ($Ba(OH)_2$, $Sr(OH)_2$ and NaOH), was high, which was responsible for the formation of $[Ti(OH)_6]^{2-}$. This, in turn, plays an important role in the formation of $BaSrTiO_3$ in an aqueous medium.

When using $BaCl_2$, $SrCl_2$ and NaOH (M1), it may be reasonable to assume that the Ti (IV) complex ion has the formulas $[TiCl_6]^{2-}$ and $[Ti(OH)_nCl_m]^{2-}$, where n and m are related with the acidity and concentration of the Cl^- ion from the salts used. In our experiment, there was a decrease in the concentration of OH^- ions in the solution, leading to a decrease in $[Ti(OH)_6]^{2-}$ formation. Thus, a competition in the formation of the intermediate species is expected.

Therefore, the nature of the salt has a direct influence on the synthesis of BST. In the present experiment, the salts of barium and strontium played an important role in the formation of the hexahydroxo titanate species ($[Ti(OH)_6]^{2-}$), which would be a determinant species in the formation of the backbone of TiO_6 octahedra.

5. Theoretical calculations

To give better support to the experimental results, with regard to the formed phase of $Ba_{1-x}Sr_xTiO_3$, we proceeded to carry out quantum chemical calculations to obtain the energetic stability and the effective charges on the atoms for materials with compositions of x=0, 0.5 and 1. To simulate the different solid compounds, the cluster methodology [34–36] was used, i.e., a finite number of atoms were used to represent the different phases of the material, as shown in Fig. 5. The energy and electronic properties were calculated by solving the Kohn–Sham equations in an atomic basis set formed by Gaussian functions. The calculations were performed using the B3LYP exchange correlation functional [37–40], which is of the hybrid type. This functional consists of a careful mix of the Hartree–Fock exchange, which is calculated with the Kohn–Sham orbitals, and the B88 exchange functional [37] plus the LYP correlation functional [40]. For titanium and oxygen atoms, the 6-31G basis set [41,42] has been used. For barium and strontium atoms, the pseudopotential of the Los Alamos group [43] with a corresponding basis set has been used. For barium atoms, the pseudopotential replaces 48 core electrons; thus, only ten valence electrons are considered. For strontium atoms, the pseudopotential replaces 28 core electrons; thus, only ten valence electrons are considered. Crystallographic data were used to represent the initial cubic phases for BT, ST and BST

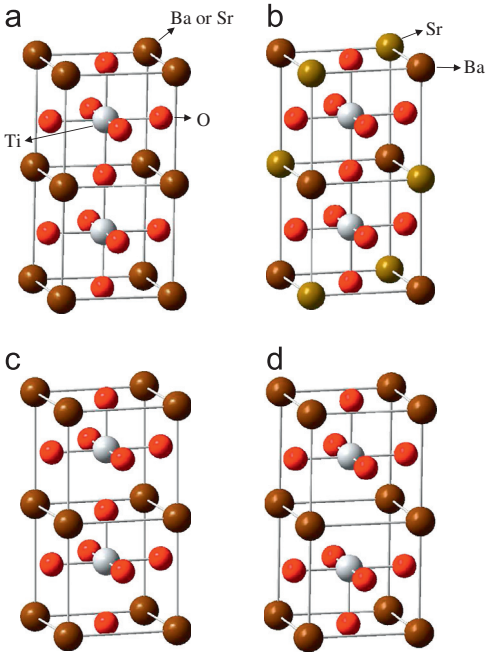

Fig. 5. Cluster model structures: (a) cubic of perovskite type, (b) cubic BST, similar to “a”, (c) tetragonal distortion and (d) oxygen vacancy.

Table 3
Effective charges (Q) and binding energies per atom (E_b) for structures: a) cubic of perovskite type, b) tetragonal distortion and c) oxygen vacancy.

Property	ST			BST			BT		
	a	b	c	a	b	c	a	b	c
Q(Ti)e	3.292	3.256	2.096	3.292	3.256	2.061	3.275	3.241	1.981
Q(O)e	−1.289	−1.333	−1.177	−1.373	−1.370	−1.201	−1.405	−1.401	−1.214
Q(Sr)e	1.510	1.513	1.631	1.538	1.541	1.655	–	–	–
Q(Ba)e	–	–	–	1.549	1.552	1.660	1.576	1.578	1.682
E_b(eV)	−19.25	−19.24	−16.56	−19.02	−19.01	−16.34	−18.81	−18.80	−16.17

reported in the literature [26,44,45]. Effective charges based on Atomic Polar Tensors (APT) were used for the discussion of the results [46]. All calculations were performed using the Gaussian 09 program [47].

The binding energy per atom for the analysis of the energetic stability for the different phases in Fig. 5 was calculated as:

$$E_b = [E(\text{phase}) - mE(\text{Ti}) - nE(\text{O}) - oE(\text{O}) - pE(\text{Sr}) - kE(\text{Ba})]/w \quad (1)$$

E(phase), E(Ti), E(O), E(Sr) and E(Ba) being the energies of the model cluster of the specific phase (cubic, tetragonal or oxygen vacancy), titanium atom, oxygen atom, strontium atom and barium atom, respectively; *m*, *n*, *o*, *p* and *k* are the specific total number of atoms considered in each cluster model, and w is the number of atoms in each cluster model.

5.1. Theoretical discussion

Fig. 5 shows the cluster models which represent the initial cubic structure of the perovskite type (a), cubic BST, showing the distribution of Ba and Sr in the structure (b), the distorted cubic structure of the tetragonal type, shifting the TiO_4 plane along the *Z*-axis by 0.1 Å (c), and the structure for oxygen vacancy (d) for compositions of $x=0$, 0.5 and 1. The effective charges and binding energies per atom are collected in Table 3. Analysis of the effective charges shows that the tetragonal distortion does not significantly affect the effective charge on the atoms in comparison with the cubic phase. Additionally, the stability of the compound is not compromised, where the binding energy suffers a variation of only 0.01 eV. The distortion of the oxygen vacancy in the structure greatly affects the stability and charge distribution, as we can see from Table 3. The titanium atom is the one that suffers the greater variation in the charge (ΔQ), between 1.196e to BST 1.231e. These results suggest that oxygen vacancies can induce a decrease in the oxidation state by almost one unit for the Ti atom. Thus, assuming that the oxidation state of Ti is +4, then the existence of Ti^{+3} induced by oxygen vacancies is possible, which is in agreement with the XPS results. On the other hand, the analysis of the binding energies shows that the structure of ST is more stable in comparison with BT, and the structure of BST has an intermediate stability among both structures. These results show that the incorporation of Sr into the structure of BT confers greater stability to the compound. In addition, the charge analysis show that in ST the charge on the oxygen and Sr atoms is slightly less negative and less positive, respectively, in comparison with oxygen and Ba atoms in BT. The incorporation of the Sr atoms into the structure of BT produces a slightly more positive charge on the Ti atoms, a less negative charge on the oxygen atoms and a less positive charge on the Ba atoms, showing that BST would tend toward the ST properties. This behaviour can be explained due to the Sr atom is slightly more electronegative than Ba (0.95 v/s 0.89, using Pauling scale).

Based on the previous results, we can conclude that deformation of the lattice structure is present in the synthesis of the compound using both methods. To clarify which is the main contribution to the structural deformation of the compound, whether the tetragonal type or oxygen vacancy, it is necessary to carry out a more detailed analysis of the microstructure.

6. Concluding remarks

The effects of two different salts of barium ($BaCl_2$, $Ba(OH)_2$) and strontium ($SrCl_2$, $Sr(OH)_2$) as the starting reactants in the synthesis of $Ba_{1-x}Sr_xTiO_3$ ($x=0,1$) nanoparticles were analysed. According to our results, different structural characteristics were produced due to the presence of anions (Cl^- and OH^-) during the synthesis of the compound. The M1 method, based on chloride ions, will have better results for Sr incorporation when the Ba:Sr mole ratio used in the reactant is <1. The mechanism is complex and requires in-depth research. On the other hand, XPS results showed a different local environment for each element in the BST. An analysis of the O 1 s signal revealed a higher presence of chemisorbed species and oxygen vacancies in the M1 method-grown samples than in the M2 method-grown ones. Finally, the theoretical calculations showed that the incorporation of Sr into the structure of BT confers great stability to the compound, and the presence of Ti with a lower oxidative state is possible due to the distortion of the lattice structure of the compound, which is most likely caused by oxygen vacancies.

Acknowledgements

This work has been partially financed by: FONDECYT Grant under contract no 1110555.

Basal Financing Program CONICYT, FB0807 (CEDENNA). MICINN Project ACPHIN (FIS2009-10150). E. C. is gratefully acknowledged for fellowship from CONICYT through Becas Chile 2010. Proyectos de la Dirección de Investigación (U. de Antofagasta), Grant DI-CODEI-2010-01.

References

[1] A. Yourdkhani, G. Caruntu, Characterization of the microstructural and piezoelectric properties of $PbTiO_3$ thin films synthesized by liquid-phase deposition, Journal of Physical Chemistry C 115 (2011) 14797–14805.
[2] Y. Man-Soon, K. Neamul Hayet, C. Byung-Ki, L. Young-Geun, U. Soon-Chul, The effect of nano-sized BNBT on microstructure and dielectric/piezoelectric properties, Ceramics International 35 (2009) 3027–3036.
[3] S. Fuentes, R. Zárate, E. Chávez, P. Muñoz, D. Díaz-Droguett, Preparation of $SrTiO_3$ nanomaterial by a sol–gel-hydrothermal method, Journal of Material Science 45 (2010) 1448–1452.
[4] J. Qi, L. Li, W. Li, Y. Wang, Z. Gui, The influence of doping style on the grain growth of $BaTiO_3$ ceramics, Material Science and Engineering B 99 (2003) 214–216.
[5] C. Zhang, Y. Jia, Y. Jing, Y. Yao, J. Ma, J. Sun, DFT study on electronic structure and optical properties of N-doped, S-doped, and N/S co-doped $SrTiO_3$, Physica B 407 (2012) 4649–4654.
[6] J.H. Qiu, Effect of domain wall on the dielectric properties of the BaTiO3/SrTiO3 superlattices, Solid State Communication 150 (2010) 1052–1055.
[7] S. Ezhilvalavan, T. Tseng, Progress in the developments of $(Ba,Sr)TiO_3$ (BST) thin films for Gigabit era DRAMs, Material Chemistry Physics 65 (2000) 227–248.
[8] J. Wang, T. Zhang, R. Pan, J. Jiang, Z. Ma, C. Xiang, Investigation on the dielectric properties of $(Ba,Sr)TiO_3$ thin films on hybrid electrodes, Materials Chemistry and Physics 121 (2010) 28–31.
[9] A. Ioachim, M. Toacsan, M. Banciu, L. Nedelcu, F. Vasiliu, H. Alexandru, C. Berbecaru, G. Stoica, Barium strontium titanate-based perovskite materials for microwave applications, Progress in Solid State Chemistry 35 (2007) 513–520.
[10] J. Jeon, Effect of $SrTiO_3$ concentration and sintering temperature on microstructure and dielectric constant of $Ba1-xSrxTiO_3$, Journal of the European Ceramics Society 24 (2004) 1045–1048.
[11] S. Lahiry, A. Mansingh, Dielectric properties of sol–gel derived barium strontium titanate thin films, Thin Solid Films 516 (2008) 1656–1662.
[12] X. Shun Hua, J. Wei Fen, L. Kun, X. Jin Hong, Z. Lin, Structure and ferroelectric properties of barium titanate films synthesized by sol–gel method, Materials Chemistry Physics 127 (2011) 420–425.
[13] J. Li, D. Jin, L. Zhou, J. Cheng, Dielectric properties of Barium Strontium Titanate (BST) ceramics synthesized by using mixed-phase powders calcined at varied temperatures, Material Letters 76 (2012) 100–102.
[14] D.S. Jung, S.K. Hong, J.S. Cho, Y.C. Kang, Morphologies and crystal structures of nano-sized $Ba1-xSrxTiO3$ primary particles prepared by flame spray pyrolysis, Materials Research Bulletin 43 (2008) 1789–1799.
[15] J. Barrel, K. MacKenzie, E. Stytsenko, M. Viviani, Development of pyroelectricceramics for high-temperature applications, Materials Science and Engineering B 161 (2009) 125–129.
[16] A.Z. Simões, F. Moura, T.B. Onofre, M.A. Ramirez, J.A. Varela, E. Longo, Microwave-hydrothermal synthesis of barium strontium titanate nanoparticles, Journal of Alloys Compounds 508 (2010) 620–624.
[17] W. Xiao, X. Gang, R. Zhaohui, W. Yonggang, S. Ge, H. Gaorong, Composition and shape control of single-crystalline $Ba1-xSrxTiO_3$ ($x=0-1$) nanocrystals via a solvothermal route, Journal of Crystal Growth 310 (2008) 4132–4137.
[18] H. Avila, L. Ramajo, M. Reboredo, M. Castro, R. Parra, Hydrothermal synthesis of $BaTiO_3$ from different Ti-precursors and microstructural and electrical properties of sintered samples with submicrometric grain size, Ceramics International 37 (2011) 2383–2390.
[19] T. Hoshina, S. Wada, Y. Kuroiwa, T. Tsurumi, Composite structure and size effect of barium titanate nanoparticles, Applied Physics Letters 93 (2008) 192914–192917.
[20] A. Sundaresan, R. Bhargavi, N. Rangarajan, U. Siddesh, C.N. Rao, Ferromagnetism as a universal feature of nanoparticles of the otherwise nonmagnetic oxides, Physical Review B. 74 (2006) 161306–161310.
[21] R. Zhang, J. Li, D. Viehland, Self-assembly of point defects into clusters and defectfree regions: a simulation study of higher-valent substituted ferroelectric perovskites, Computer Material Science 29 (2004) 67–75.
[22] I. Fujii, M. Ugorek, S. Trolier-McKinstry, Grain size effect on the dielectric nonlinearity of $BaTiO_3$ ceramics, Journal of Applied Physics 107 (2010) 104116–104121.
[23] P. Dutta, R. Asiaie, S. Akbar, W. Zhug, Hydrothermal synthesis and dielectric properties of tetragonal $BaTiO_3$, Chemistry of Materials 6 (1994) 1542–1548.
[24] K. Razak, A. Asadov, J. Yoo, E. Haemmerle, W. Gao, Structural and dielectric properties of barium strontium titanate produced by high temperature hydrothermal method, Journal of Alloys and Compounds 449 (2008) 19–23.
[25] M.S Zhang, J. Yu, W. Chen, Z. Yin, Optical and structral properties of pure and Ce-doped nanocrystals of barium titanate, Progress in Crystal growth and Characterization of Materials 40 (2000) 33–42.
[26] E. Chávez, S. Fuentes, R. Zárate, L. Padilla-Campos, Structural analysis of nanocrystalline $BaTiO_3$, Journal of Molecular Structure 984 (2010) 131–136.
[27] D. Ehre, H. Cohen, V. Lyahovitskaya, I. Lubomirsky, X-ray photoelectron spectroscopy of amorphous and quasiamorphous phases of $BaTiO_3$ and $SrTiO_3$, Physical Review B 77 (2008) 184106–184112.
[28] C. Xu, Y. Xia, Z. Liu, X. Meng, Chemical states change at (Ba,Sr)TiO3/Pt interfaces investigated by X-ray photoelectron spectroscopy, Journal of Physics D: Applied Physics 42 (2009) 085302–085310.
[29] J.X. Liao, C. Yang, Z. Tian, H. Yang, L. Jin, The influence of post-annealing on the chemical structures and dielectric properties of the surface layer of $Ba0.6Sr0.4TiO_3$ films, Journal of Physics D: Applied Physics 39 (2006) 2473–2478.
[30] S. Nasser, X-ray photoelectron spectroscopy study on the composition and structure of $BaTiO_3$ thin films deposited on silicon, Applied Surface Science 157 (2000) 14–22.
[31] M. Enhessari, A. Parviz, K. Ozaee, H. Abyaneh, Synthesis and characterization of barium strontium titanate (BST) micro/nanostructures prepared by improved methods, International Journal of Nano Dimension 2 (2011) 85–103.
[32] N. Pramanik, B. Ahn, S. Seok, Effects of reactant concentration and $OH-$ ions on the formation of nanocrystalline $BaTiO_3$ in solution, Materials Research Bulletin 42 (2007) 497–504.
[33] W. Zhong, C. Xia, E. Shi, B. Wang, W. Li, S. Hua, Formation mechanism of barium titanate nanocrystais under hydrothermal conditions, Science in China Series E-Engineering and Materials Science 40 (1997) 479–488.
[34] T.A. Kaplan, S.D Mahanti, Electronic Properties of Solids using Cluster Methods, Plenum Press, New York, 1995.
[35] L. Padilla-Campos, P. Fuentealba, Theoretical study of the adsorption of oxygen on a Cu(100) surface and the coadsorption with alkali atoms, Theoretical Chemistry Accounts 110 (2003) 414–420.
[36] L. Padilla-Campos, A theoretical investigation of occupation sites for tritium atoms in lithium titanate, Journal of Molecular Structure (Theochem) 621 (2003) 107–112.
[37] A.D. Becke, Density-functional thermochemistry. III. The role of exact exchange, Journal of Chemical Physics 98 (1993) 5648–5653.
[38] A.D. Becke, Density-functional exchange-energy approximation with correct asymptotic behavior, Physical Review A 38 (1988) 3098–3100.
[39] B. Miehlich, A. Savin, H. Stoll, H. Preuss, Results obtained with the correlation energy density functionals of becke and Lee, Yang and Parr, Chemical Physics letters 157 (1989) 200–206.
[40] C. Lee, W. Yang, G.R. Parr, Development of the Colle-Salvetti correlation-energy formula into a functional of the electron density, Physical Review B 37 (1988) 785–789.
[41] W.J. Hehre, R. Ditchfield, J.A. Pople, Self-consistent molecular orbital methods. XII. further extensions of Gaussian-type basis sets for use in

molecular orbital studies of organic molecules, Journal of Chemical Physics 56 (1972) 2257–2261.
[42] V. Rassolov, J.A. Pople, M. Ratner, T.L Windus, 6-31G* basis set for atoms K through Zn, Journal of Chemical Physics 109 (1998) 1223–1230.
[43] P.J. Hay, W.R. Wadt, Ab initio effective core potentials for molecular calculations. Potentials for the transition metal atoms Sc to Hg, Journal of Chemical Physics 82 (1985) 270–284.
[44] S. Piskunov, E.A. Kotomin, D. Fuks, S. Dorfman, Ab initio calculations of the atomic and electronic structure of layered Ba0.5 Sr0.5TiO_3 structures, Materials Science and Engineering B 118 (2005) 15–18.
[45] S.Y. Kuo, W.Y. Liao, W.F. Hsieh, Structural ordering transition and repulsion of the giant LO-TO splitting in polycrystalline BaxSr1-$x$$TiO_3$, Physical Review B 64 (2001) 224103–224110.
[46] J. Cioslowski, A new population analysis based on atomic polar tensor, Journal of the American Chemical Society 111 (1989) 8333–8336.
[47] M.J. Frisch, G.W. Trucks, H.B. Schlegel, G.E. Scuseria, M.A. Robb, J.R. Cheeseman, G. Scalmani, V. Barone, B. Mennucci, G.A. Petersson, H. Nakatsuji, M. Caricato, X. Li, H.P. Hratchian, A.F. Izmaylov, J. Bloino, G. Zheng, J.L. Sonnenberg, M. Hada, M. Ehara, K. Toyota, R. Fukuda, J. Hasegawa, M. Ishida, T. Nakajima, Y. Honda, O. Kitao, H. Nakai, T. Vreven, J.A. Montgomery, Jr., J.E. Peralta, F. Ogliaro, M. Bearpark, J.J. Heyd, E. Brothers, K.N. Kudin, V.N. Staroverov, T. Keith, R. Kobayashi, J. Normand, K. Raghavachari, A. Rendell, J.C. Burant, S.S. Iyengar, J. Tomasi, M. Cossi, N. Rega, J.M. Millam, M. Klene, J.E. Knox, J.B. Cross, V. Bakken, C. Adamo, J. Jaramillo, R. Gomperts, R.E. Stratmann, O. Yazyev, A.J. Austin, R. Cammi, C. Pomelli, J.W. Ochterski, R.L. Martin, K. Morokuma, V.G. Zakrzewski, G.A. Voth, P. Salvador, J.J. Dannenberg, S. Dapprich, A.D. Daniels, O. Farkas, J.B. Foresman, J.V. Ortiz, J. Cioslowski, and D.J. Fox, Gaussian 09, Revision B.01, Gaussian, Inc., Wallingford CT, 2010.